Behaviour of Spherical Cap Bubbles in Liquid Metals

by
W. G. Davenport, A. V. Bradshaw, and F. D. Richardson

(Manuscript first received 17 February 1967 and, in its final form, 23 June 1967.
Professor Bradshaw and Professor Richardson are, respectively, Professor of Applied Metallurgy and Professor of Extraction Metallurgy at the Imperial College of Science and Technology, London. Dr Davenport is Assistant Professor of Metallurgy at McGill University, Montreal, Canada.)

Journal of The Iron and Steel institute, October 1967, page 1034–1042.

Abstract

Measurements have been made of the rising velocities and shapes of spherical cap bubbles of nitrogen, $1\,\mathrm{cm}^3$ and greater, rising in mercury. The results are similar to those obtained previously with water, except that the higher surface tension of mercury increases the radius of curvature at the bubble's trailing edge. Experiments with bubbles of nitrogen and oxygen in molten silver have given similar velocities, and have shown that the mass transfer coefficient of oxygen into the metal is $0.055\,\mathrm{cm\,s^{-1}}$.

LIST OF SYMBOLS

A	area of a sphere having the same volume as the bubble
$AW\,[\mathrm{O}]$	atomic weight oxygen
a	basal radius of spherical cup bubble
B	increase in pressure (atm) per unit depth of fluid ($\mathrm{atm\,m^{-1}}$)
C	concentration
$\mathscr{D}$	diffusion coefficient
f	frequency, cycles s^{-1}
g	acceleration due to gravity
H	depth below surface of zero pressure
H_I	initial depth below surface of zero pressure

H_T	depth below surface of zero pressure at the liquid surface
h	head of liquid
h_I	initial head of liquid on bubble at time of release
h_p	height of bubble measured by probe
h_a	height of spherical cap bubble through vertical axis
h_0	starting depth for velocity measurement
K	equilibrium coefficient $= \frac{[\%\mathrm{C}][\%\ \mathrm{O}]}{p_{\mathrm{CO}}}$, wt-% and atm equal 0.002 at 1600 °C
k_L	liquid phase mass-transfer coefficient
M	constant
N	number of cycles
n	moles of gas, O_2 or CO, in bubble
P	pressure in bubble
P_T	constant top pressure in column for velocity measurements
p	atmospheric pressure above the liquid surface while bubble is rising, atm
p_C	pressure in column above liquid surface after the introduction of bubble into the cup, atm
p_f	final pressure in column above liquid surface when bubble has just reached surface, atm
p_I	initial pressure in column above liquid surface before introduction of bubble, atm
q	SIEVERT's Law constant
$\mathscr{R}$	gas constant
R_c	radius of curvature of front of spherical cap bubble
R_E	radius of curvature of trailing edge of bubble
r	horizontal displacement of probe from axis of a spherical cap bubble
r_e	equivalent radius, i.e. radius of a sphere having the same volume as the bubble
S	shape factor $= \frac{A}{V^{\frac{2}{3}}} = (36\pi)^{\frac{2}{3}}$
T	transit time of bubble through h_0, cm
t	time
U	rising velocity of bubble
U_∞	rising velocity of bubble in fluid of infinite extent
U_s	surface velocity
V	bubble volume

V_{AV}	arithmetic average of bubble volume at h_0, and at top of column
V_I	initial bubble volume on release
V_T	volume of bubble at top of column used in velocity measurements
w	exponent
α	half-angle subtended by the bubble at the centre of curvature
γ	surface tension
θ	absolute temperature
ν	volume of enclosed space in column above liquid surface before the introduction of bubble
ρ	density of fluid
b	in bulk liquid
i	at liquid inreface

1. INTRODUCTION

Many metallurgical processes depend upon the behaviour of gas bubbles rising through liquid metals. Examples are provided by the removal of carbon during steelmaking, vacuum degassing, and inert gas flushing. In such processes, substances dissolved in the metals are removed by the gas. Three steps are involved in the transfer from one phase to the other: transport of the dissolved species to the bubble interface, chemical reaction in the interface, and finally desorption as gaseous molecules. At the temperature of interest in steelmaking, the chemical and desorption steps in gas-metal processes are likely to proceed with such rapidity that transport of the solutes, present in the metal, to the bubble interface, becomes the most important of the rate-controlling factors, except where nucleation phenomena are restrictive.

There are no reported experiments from which it is possible to calculate mass transfer coefficients between metals and rising bubbles with any accuracy. One can, however, make one or two interesting estimates. Pehlke and Bement, [16], studied the rate of removal of hydrogen from aluminium at 700 °C by injecting bubbles of argon ($0.03\,\mathrm{cm}^3$ to $0.05\,\mathrm{cm}^3$) into melts 20 cm deep, at rates of $30\,\mathrm{bubbles\,s^{-1}}$ to $60\,\mathrm{bubbles\,s^{-1}}$. Assuming the bubbles to be spherical, one may calculate that the mass transfer coefficients varied from $3.7 \times 10^{-2}\,\mathrm{cm\,s^{-1}}$ to $6.8 \times 10^{-2}\,\mathrm{cm\,s^{-1}}$ increasing with the rate of bubbling. From the observations made by Brower and Larsen, [7],[6], on a gently boiling open hearth, Richardson, [17], has estimated the mass transfer coefficient for

the spherical cap bubbles to be about $5 \times 10^{-2}\,\mathrm{cm\,s^{-1}}$, but this calculation needs revision, as indicated below.
In metallurgical processing, one is mainly concerned with bubbles which have volumes greater than $5\,\mathrm{cm}^3$, and which adopt the spherical cap shape shown in Figure 1. In a previous investigation, [8], the authors studied the behaviour of such bubbles in aqueous media and other liquids of low density. In the present study, experiments have been made with liquid metals. The shapes and rates of rise of spherical cap bubbles have been measured in liquid mercury, and rates of rise and mass transfer coefficients for oxygen have been investigated in liquid silver. Silver was chosen because of its relatively low melting point, its high oxygen solubility, and the absence of any oxide phase when molten silver and oxygen are in contact. At present, it seems too difficult to conduct such experiments with liquid iron.

2. EXPERIMENTAL

2.1. Investigation using mercury

Studies on the shapes and velocities of bubbles rising in mercury were carried out in a Perspex tube (15 cm i.d. by 90 cm long). Single bubbles were formed by injecting gas into an inverted cup, which was then rotated by hand to release the bubble in a manner described elsewhere for experiments with water, [8]. Measurement of the amounts of gas displaced above the liquid column into a soap film meter permitted the bubble volumes to be determined with a standard deviation of $\pm 0.02\,\mathrm{cm}^3$. The velocities were calculated by the time taken for the bubble to rise through a known depth of mercury. This was measured on a stopwatch (0.01 s catchment) which was started automatically by the rotation of the cup. The watch was stopped when the disturbance of the mercury surface, due to the bubble breaking through, interrupted a beam of light directed at a photoelectric cell. In mercury, visual observations could not be used to determine the exact time of release of the bubble from the cup. Thus, an initial series of experiments was made to determine the time between the cup reaching a 45° angle of tilt (when the bubble probably leaves), and the bubble breaking the surface after rising through 16.2 cm of mercury measured from the base of the cup. This was followed by the main experiments conducted in a column of mercury 64.4 cm deep. The velocities were calculated from the differences between the times required in the 64.4 cm column and the mean value in the short column. In this way, inaccuracies in the measurement of the exact time of release were eliminated.

The shapes of the bubbles in mercury were measured by means of electrical probes. The maximum radius in a horizontal plane was measured by a series of 20 probes (0.05 cm o.d.) arranged in the form of a cross, as shown in Figure 2(b). Each probe (see Figure 2(a)) was insulated with enamel, except

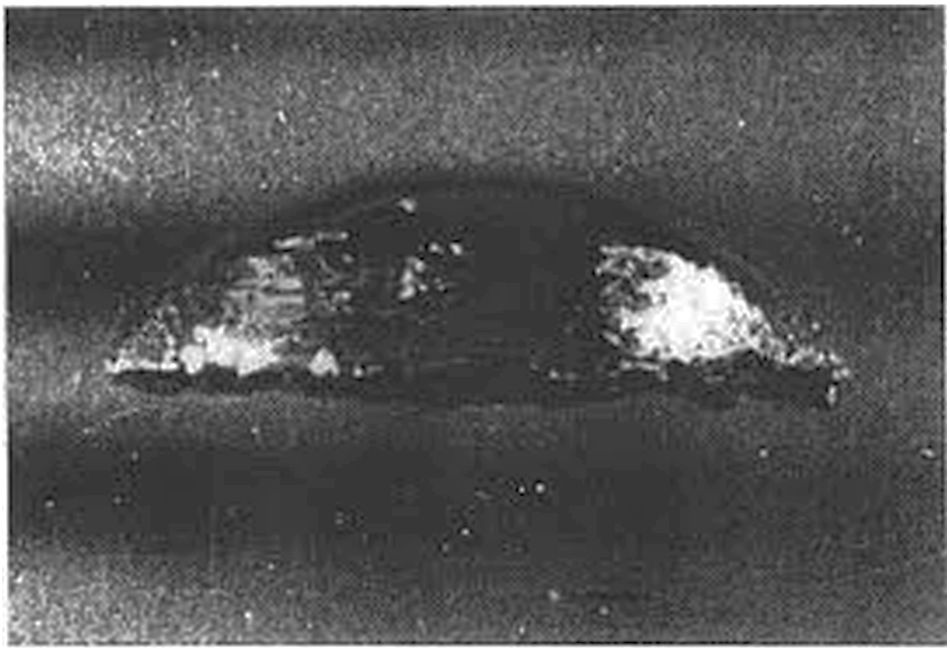

Figure 1: Typical $40\,\mathrm{cm}^3$ spherical cap bubble rising in water

for its extreme tip. As long as this remained in contact with mercury, the circuit was closed and the indicating lamp was alight. If the passage of an air bubble broke the circuit, the lamp was extinguished, and remained so even after the bubble had passed, since the initial interruption of the circuit also tripped a reed switch (response time $8 \times 10^{-4}\,\mathrm{s}$). A permanent record of the probes which had been in contact with a bubble was thus obtained. After each experiment, the reed switches were all closed magnetically. Distortion of the bubble by the probes was reduced by adjusting them to be near the rim as shown in Figure 2(b).

The heights of the bubbles were measured by a single probe (Figure 2(c)), located centrally with respect to the cross of probes just described. Through this central probe, an alternating current of $1000\,\mathrm{C\,s^{-1}}$ was passed. A pulse-counter was arranged in parallel with the probe, but it was effectively short-circuited except when the tip of the probe was inside a gas bubble. The number of cycles passing through the counter was measured for each bubble, so that the time taken for the bubble to advance a distance equal to its own thickness, at the point of penetration of the probe, was known. The value of this thickness was then calculated from this time and the rising velocity.

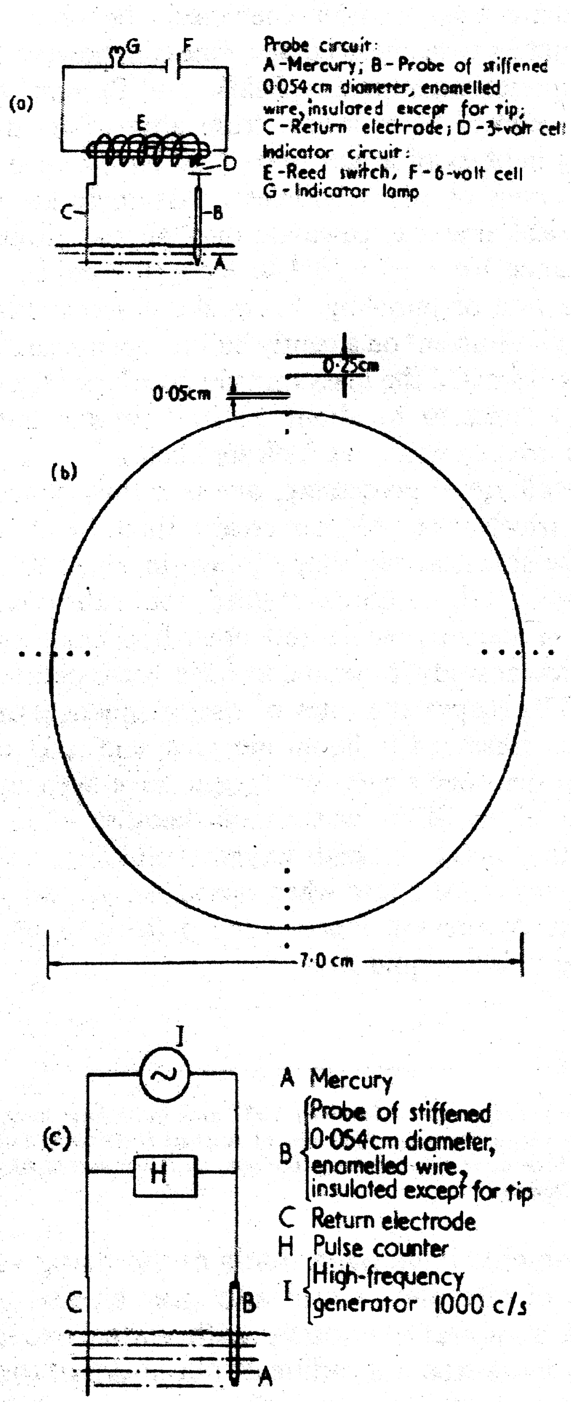
(a)
G
F
E
D
C
B
A
Probe circuit:
A - Mercury; B - Probe of stiffened 0·054 cm diameter, enamelled wire, insulated except for tip;
C - Return electrode; D - 3-volt cell
Indicator circuit:
E - Reed switch, F - 6-volt cell
G - Indicator lamp
(b)
0·05cm
0·25cm
7·0 cm
(c)
I
H
C
B
A
A Mercury
B Probe of stiffened 0·054cm diameter, enamelled wire, insulated except for tip
C Return electrode
H Pulse counter
I High-frequency generator 1000 c/s

Figure 2: Electronic circuits for measuring bubble shape
(a) – one of a series of probe circuits used for measuring basal radius; (b) – typical arrangement of probes (position of probes shown by ······ superimposed on plan of 40 mL bubble); (c) – single probe circuit for bubble height

2.2. Investigation with silver

The apparatus (Figure 3) was designed to operate at 1000 °C, and at this temperature the silver could be held satisfactorily in "Nimonic 75" (80 % Ni–20 % Cr). Temperature measurements indicated a variation of less than 10 °C over the length of the column. Single bubbles were produced by a rotating cup similar to that used in the investigation with mercury. In order to prevent leakage of silver around the shaft of this cup, high-temperature packing, consisting of a mixture of alumina powder and silica fibre, was used. The use of a soap film meter to measure changes in volume was inconvenient for this high-temperature investigation. In consequence, changes of pressure were measured instead, and the top of the column was sealed by a threaded plug screwed to a nickel washer. Pressure measurements were carried out with a mercury pressure gauge (0.35 cm i.d.), and, as only very small quantities of gas passed from the furnace into the pressure gauge, the entire system could be considered isothermal. Since it was necessary to know the volume of the space in the column above the liquid silver, the distance between the top of the column and the liquid surface was measured to an accuracy of ±2 % by an electrical contact device attached to a micrometer.

Velocities of nitrogen bubbles rising in silver were obtained from a cinematograph record of pressure changes indicated by the pressure gauge. These velocities were in the absence of mass transfer, since experiments at pressures up to 450 atm have shown nitrogen to be virtually insoluble in molten silver, [3]. Rates of mass transfer from oxygen bubbles into molten silver were also obtained by measuring pressure changes as a function of time.

Preliminary experiments on mass transfer indicated that the transfer of oxygen from gas into silver containing no oxygen was too rapid to be measured by the method devised. Satisfactory measurements were, however, made on transfer to silver which contained oxygen at a concentration of $1.87(4) \times 10^{-3}$ g atom cm^{-3}. These solutions were made by bubbling a slow stream of gas of 93 % O_2 and 7 % N_2 for some hours through the silver in the column. Pure oxygen was then bubbled vigorously through the metal for a short period to flush out nitrogen remaining in the top of the column, and mix the metal thoroughly. The column was then closed. The top pressure rose to 1.120(25) atm due to the evolution of a small amount of oxygen from the metal. From this pressure, the concentration given above was derived, [11]. This concentration remained virtually constant throughout the transfer experiments, because the quantity introduced by each bubble was negligible compared with the quantity already in the silver. Before introducing oxygen into the cup, the top pressure was adjusted to atmospheric pressure or slightly below. The system was then sealed, the oxygen was introduced, and the bubble quickly released. During its rise, pressure changes were recorded on a cine camera.

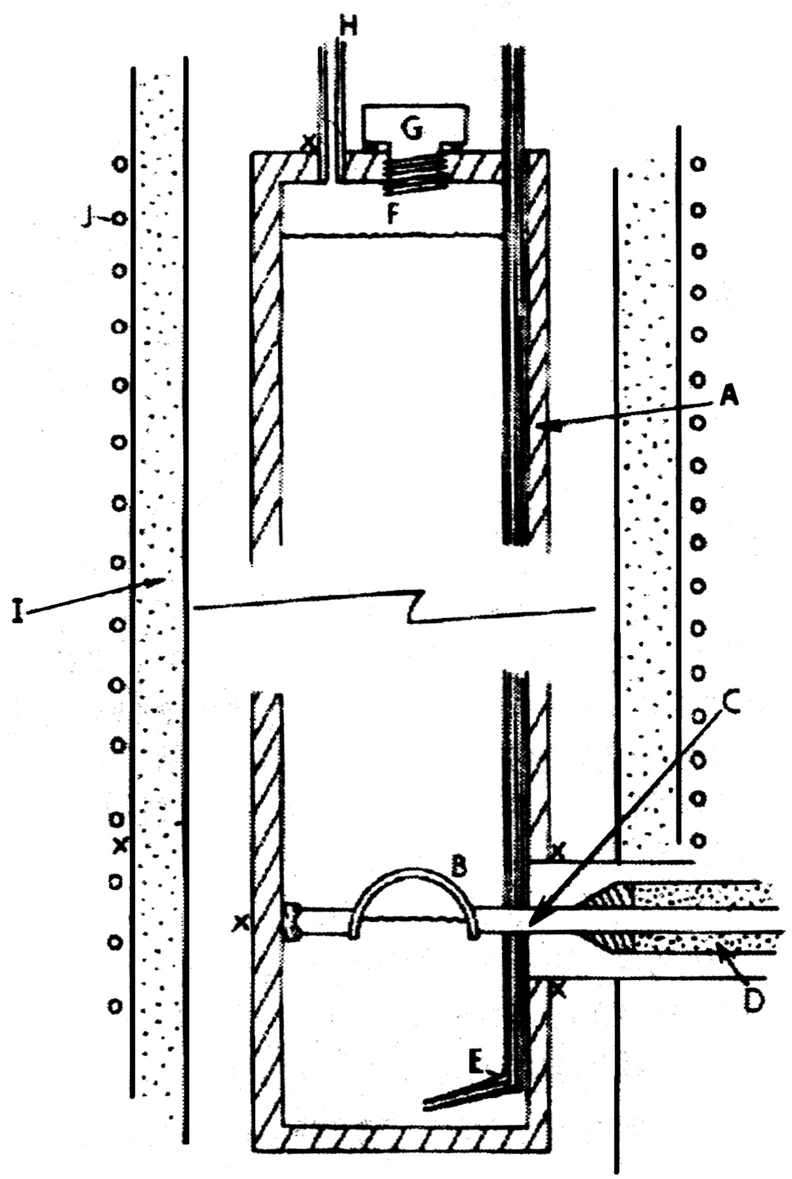

Figure 3: Apparatus for measuring velocities and mass transfer coefficients in molten silver

A – cylinder 60 cm high, 7.6 cm, made from Nimonic 75 alloy
B – Nimonic alloy cup
C – shaft for rotating cup
D – kept under pressure
E – gas inlet to cup
F – gas space above silver
G – plug
H – outlet to manometer
I – furnace insulation (vermiculite arc alumina)
J – Kanthal "A" furnace wiring, suitable for 25 kW
X – positions of Pt/Pt-3 % Rh thermocouples

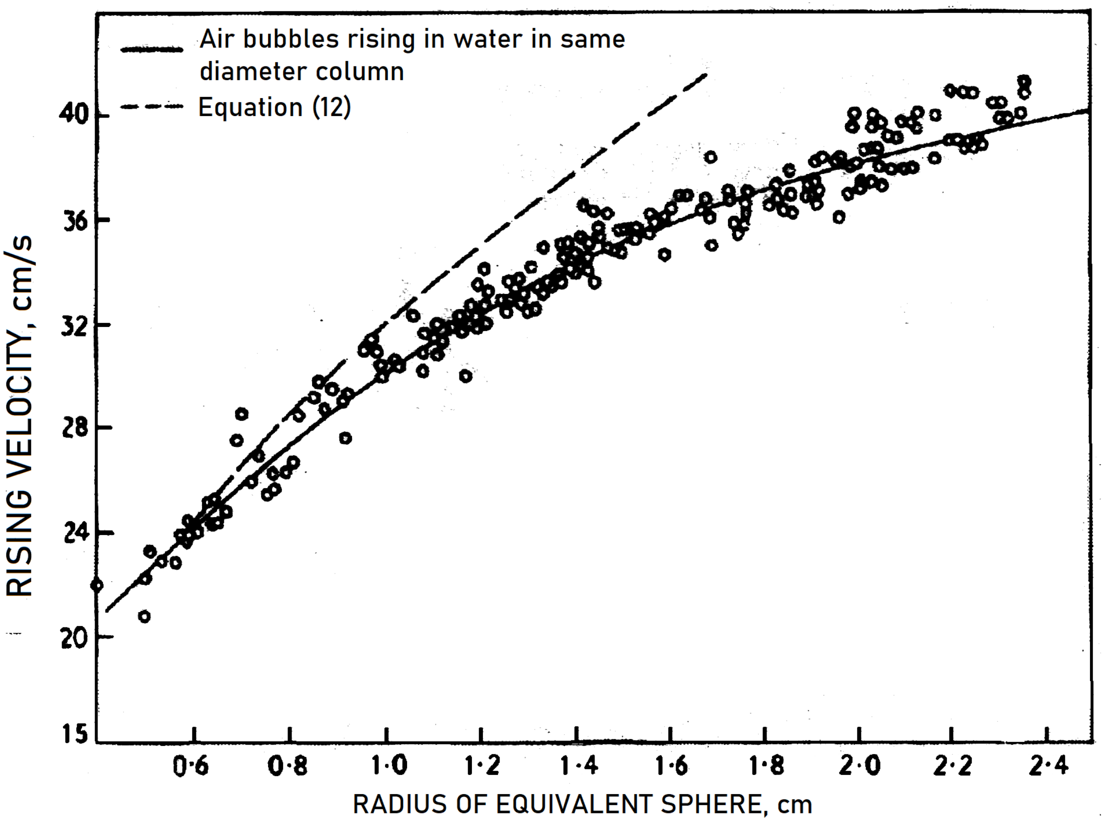

Figure 4: Velocities of air bubbles rising through 48.2 cm of mercury in 15 cm diameter column

3. RESULTS

3.1. Mercury Investigation

3.1.1. Rising Velocities

The mean velocities, calculated from the total time required for the bubble to rise through the mercury, are plotted against the radius of a sphere having the same volume as the bubble, known as the equivalent radius (Figure 4). The mean scatter of points about the curve is ±5 % on the velocity.

A rising bubble expands due to the decrease in static pressure. For the purposes of the graph, therefore, the bubble volume used as a basis for calculating the equivalent radius has been taken as the arithmetic mean of the volume at the top of the column, and at 48.2 cm (i.e. 64.4 cm to 16.2 cm) below the surface. As shown in the Appendix, the difference between the equation of the curve in Figure 4, and that relating the instantaneous velocity and radius, is trivial, and does not exceed 3 %.

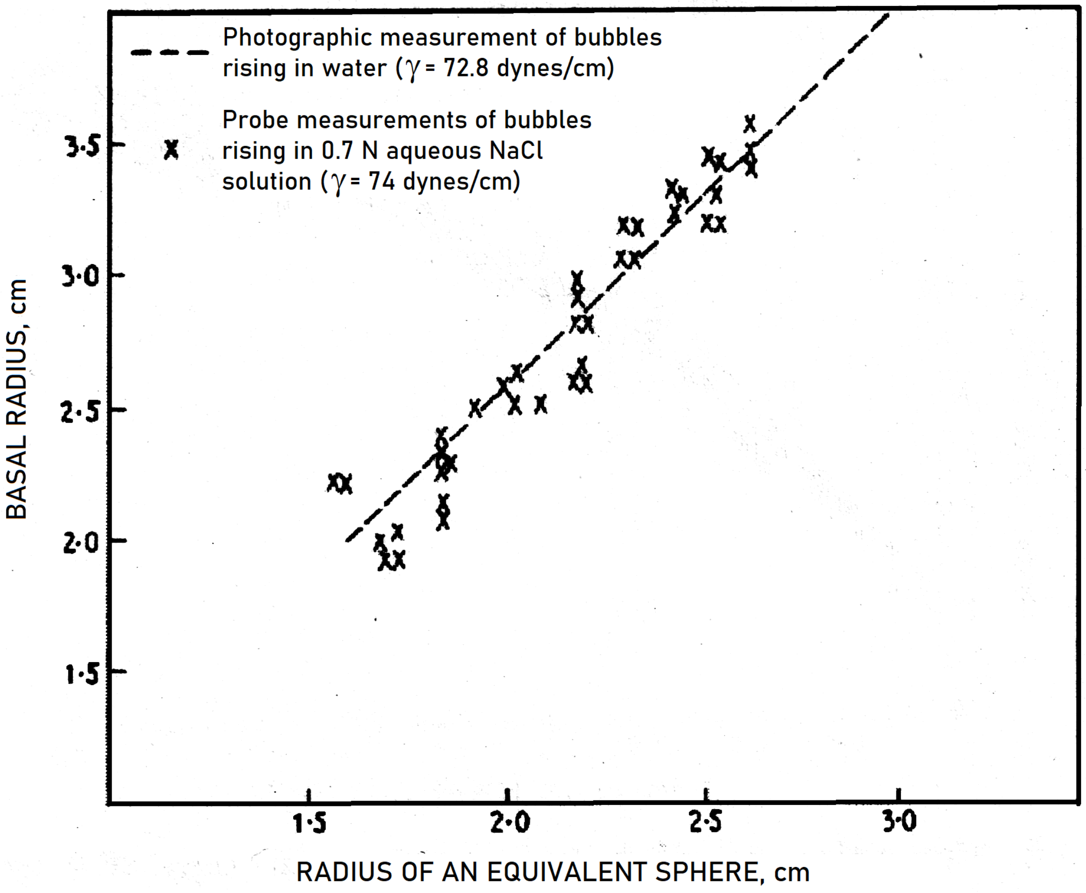

Figure 5: Comparison of probe and photographic measurements of basal radii of spherical cap bubbles

3.1.2. Bubble Shapes

The suitability of probes for measuring the basal radii of spherical cap bubbles was tested by carrying out preliminary experiments in an aqueous NaCl solution, and comparing the results with those obtained from photographs of similar bubbles rising in water. The results, which are shown in Figure 5, confirm that the probe measurements are reliable.

The basal radius of each bubble was obtained from a circle of best-fit encircling the four outermost probes interrupted by the bubble. The height of the bubble at the probe position (h_p) was calculated from:

$$h_p = \frac{U \cdot N}{f} \,. \tag{1}$$

h_p may then be substituted in the equation for a spherical surface to give

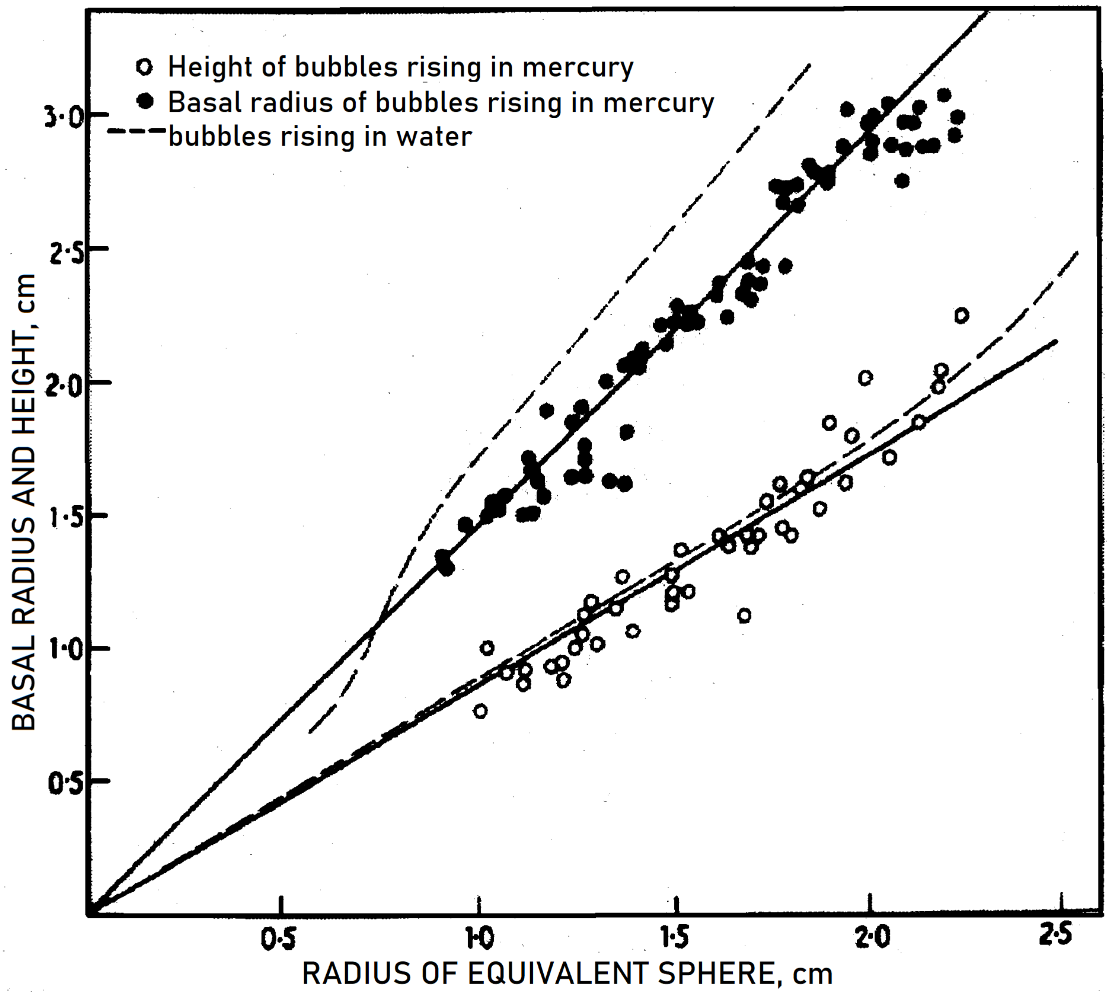

Figure 6: Heights and basal radii of rising bubbles as function of equivalent radius

the height of the bubble at the vertical axis h_a:

$$a^2 \cdot \frac{h_p}{h_a} - h_p h_a = a^2 - \left(r^2 + h_p^2\right) \tag{2}$$

The axial displacement of the probe r was determined from measurements obtained with the cruciform arrangement of the probes. The results of the shape measurements are shown in Figure 6.

3.2. Silver Investigation

3.2.1. Relation Between Bubble Volume and Top Pressure

The volume of a bubble V within the metal held in the apparatus shown in Figure 3, may be related to the volume ν above the metal before the introduction of gas into the cup, and the pressures recorded by the pressure gauge by the equation:

$$V = \nu \cdot \left(1 - \frac{p_I}{p}\right) \tag{3}$$

The slight change in the volume of the top space caused by the change in pressure gauge level as the bubble rises is negligible compared with the initial volume ($\nu \approx 120\,\mathrm{cm}^3$).

The final top pressure after the rise of an inert bubble may be calculated from:

$$p_f = p_c + Bh_I \cdot \left(1 - \frac{p_I}{p_c}\right) \tag{4}$$

Measurements of $p_f - p_c$ recorded by the pressure gauge have been compared with Equation 4 in order to check the accuracy of the measuring technique: the values obtained are within ±6 % of those predicted by Equation 4.

The interpretation of the volume changes during the bubble rise is somewhat difficult, owing to inertial effects associated with the mercury pressure gauge. Figure 7 shows a typical curve of pressure gauge readings for the rise of an inert gas bubble. The pressure when the bubble reaches the top of the column p_f is assumed to be the same as the final pressure shown on the pressure gauge after the oscillations have damped down.

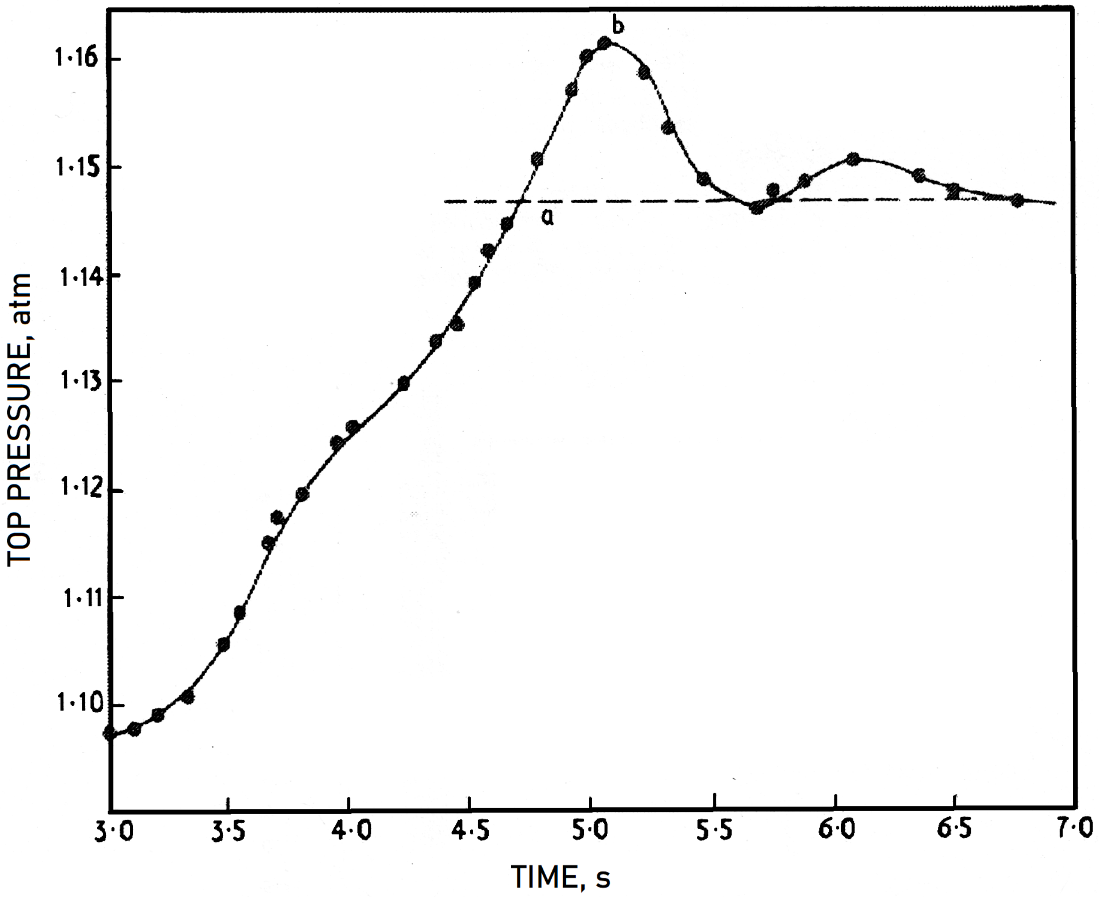

Figure 7: Curve of manometer readings versus time of rise for a 13 cm^3 bubble of inert gas in molten silver; bubble has reached top of silver at "a"; subsequent rise in reading to a maximum at "b" is due to inertial effects in the manometer

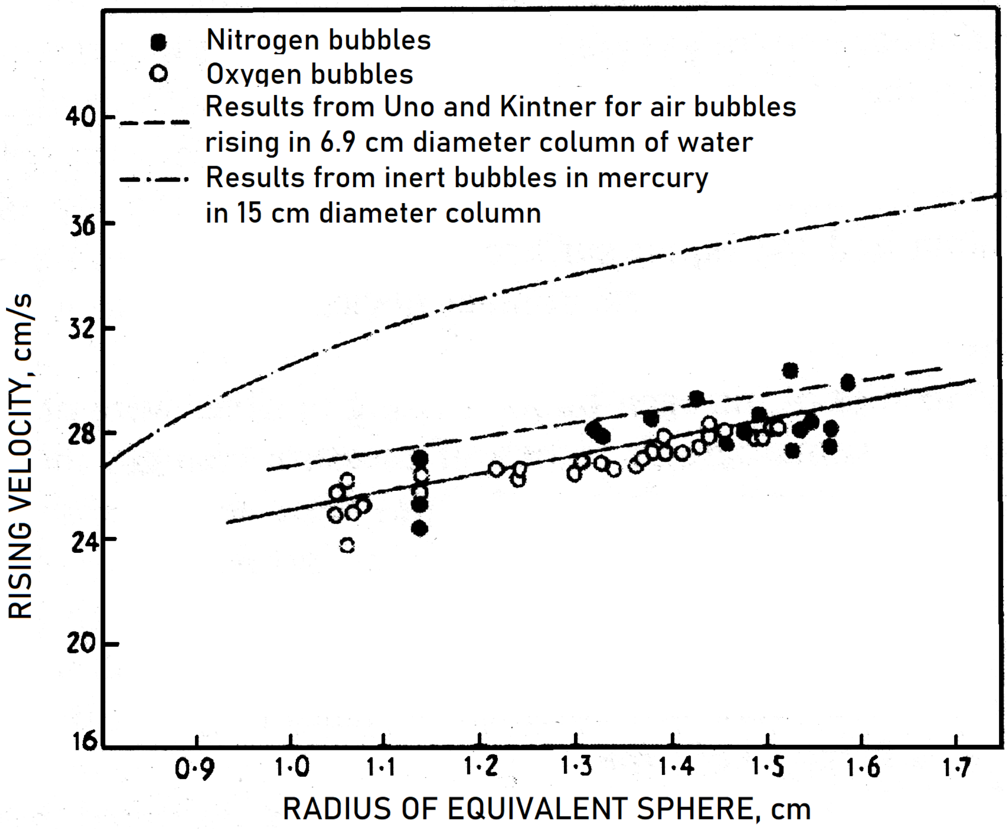

Figure 8: Rising velocities of bubbles in molten silver (1010 °C), column height 53.5 cm, diameter 7.6 cm

3.2.2. Velocity

The inertial effects in the pressure gauge made precise estimation of the velocities difficult. If these effects are the same at the start and finish of the pressure gauge movement, the total time of rise is the interval between the initial pressure gauge movement and the peak pressure (point b, Figure 7). Velocities calculated on this basis are given in Figure 8. Alternatively, there might be no lag in the initial movement of the pressure gauge; the velocity should then be calculated from the time between the initial movement of the pressure gauge and the first instant at which the final pressure is reached (point a, Figure 7). Velocities calculated in this way would be some 10 % to 15 % greater than those shown in Figure 8.

3.2.3. Mass Transfer Coefficients

The rates of absorption of oxygen by molten silver have been interpreted in terms of a liquid phase mass transfer coefficient, k_L, which is defined by the following equation:

$$\frac{\mathrm{d}n}{\mathrm{d}t}(\mathrm{O_2}) = \frac{1}{2} k_L A \cdot \left(C\,[\mathrm{O}]_b - C\,[\mathrm{O}]_i \right) . \tag{5}$$

The numerical coefficient of $\frac{1}{2}$ appears because the diatomic oxygen gas molecule is absorbed in the silver as atoms.

Equation 5 may be written in terms of pressure and volume changes in the bubble to give:

$$P \cdot \frac{\mathrm{d}V}{\mathrm{d}t} + V \cdot \frac{\mathrm{d}P}{\mathrm{d}t} = \frac{1}{2} k_L S V^{\frac{2}{3}} \mathscr{R} \theta \cdot \left(C\,[\mathrm{O}]_b - C\,[\mathrm{O}]_i \right) . \tag{6}$$

From Sievert's Law $C\,[\mathrm{O}]_i = q \cdot \sqrt{P}$; also from Equation 3:

$$\frac{\mathrm{d}V}{\mathrm{d}t} = \frac{\nu p_I}{p^2} \cdot \frac{\mathrm{d}p}{\mathrm{d}t} . \tag{7}$$

The pressure in the bubble is given by:

$$P = p + B \cdot h \tag{8}$$

and hence, since $\frac{\mathrm{d}h}{\mathrm{d}t} = -U$,

$$\frac{\mathrm{d}P}{\mathrm{d}t} = \frac{\mathrm{d}p}{\mathrm{d}t} - B \cdot U . \tag{9}$$

By the substitution of Equation 3, Equation 7, Equation 8 and Equation 9 in equation Equation 6, it is possible to obtain:

$$\begin{aligned} &\left(1 + \frac{p_I}{p^2} \cdot Bh \right) \cdot \nu^{\frac{1}{3}} \cdot \frac{\mathrm{d}p}{\mathrm{d}t} - \nu^{\frac{1}{3}} \cdot \left(1 - \frac{p_I}{p} \right) \cdot BU = \frac{1}{2} k_L S \mathscr{R} \theta \cdot \left(1 - \frac{p_I}{p} \right)^{\frac{2}{3}} \\ &\cdot \left(C\,[\mathrm{O}]_b - q \cdot [p - Bh]^{\frac{1}{3}} \right) . \end{aligned} \tag{10}$$

In Equation 10:

$$h = h_I - \int_0^t U \,\mathrm{d}t .$$

Consequently, the mass transfer coefficient can be calculated in terms of p, $\frac{\mathrm{d}p}{\mathrm{d}t}$, the rising velocity U, and the time t after release.

A typical pressure curve for a rising bubble, in which mass transfer of oxygen is occurring, is shown in Figure 9. Initially, the expansion of the bubble due to the decreasing head of silver is less than the contraction due to oxygen absorption, and there is a drop in the top pressure. Subsequently, as the bubble rises in the column, the effects are reversed and the pressure increases. In consequence, a minimum value of the pressure is obtained. In

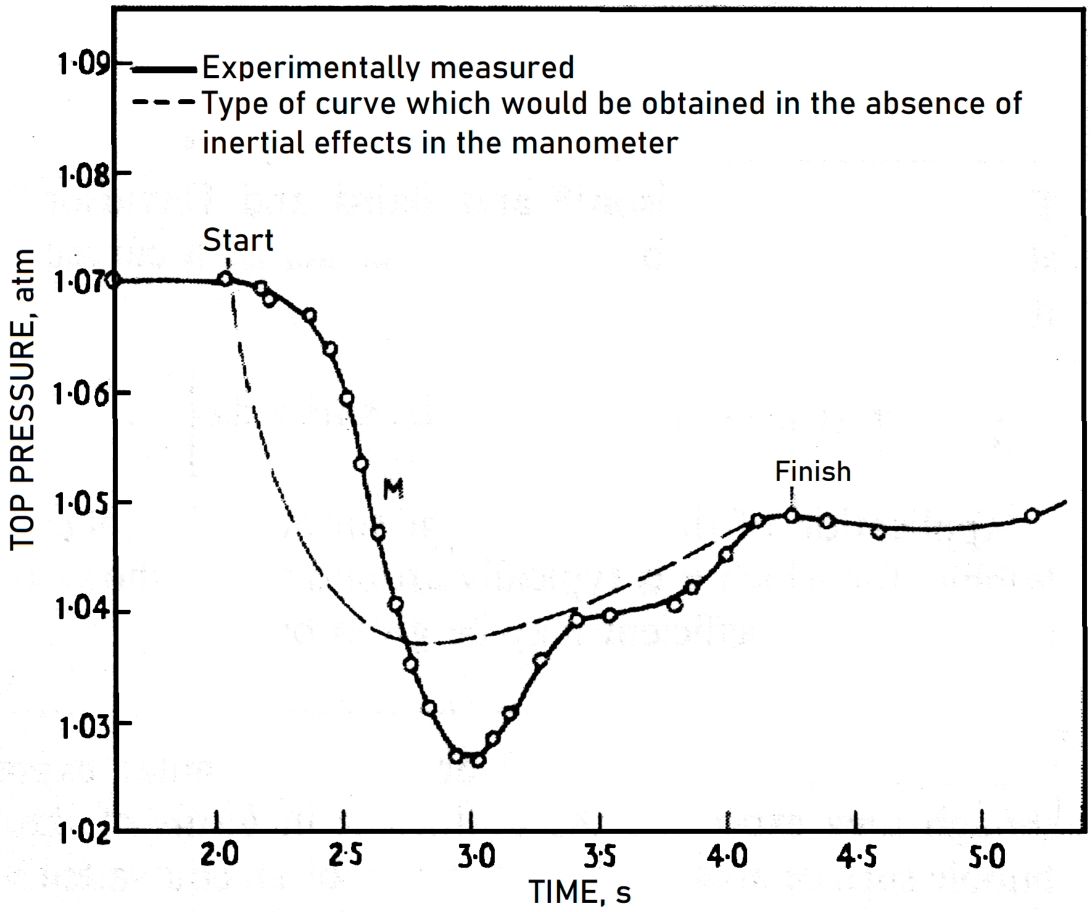

Figure 9: Typical curve of top pressure versus time for oxygen bubble (volume in cup = $13\,\text{cm}^3$) rising in molten silver, (1008 °C)

the particular example shown (Figure 9), the initial pressure in the top of the column p_I was 1.07 atm, corresponding to an initial bubble pressure P of 1.56 atm. The final bubble pressure, as it broke the surface, would be the same as that in the top space, 1.05 atm. Since the bulk oxygen concentration corresponded to an equilibrium pressure of 1.12 atm, oxygen was transferred from the bubble in the lower part of the column, and in the reverse direction in the top.

In order to minimize the oxygen transferred directly from the silver to the gas in the top of the column, each experiment was carried out as rapidly as possible. The observed rate of change of pressure in the space above the silver was only $0.001\,\text{atm}\,\text{s}^{-1}$. The bubbles rose in about 2 s, so the influence of this pressure change on the results has been neglected. The rates of mass transfer have been calculated from the pressure versus time curves in the region of constant slope (point "M" in Figure 9). Errors due to inertial effects in the pressure gauge are likely to be a minimum in this region. The velocity in Equation 10 is assumed to be that obtained at point "M" and the term $\int_0^t U \, \mathrm{d}t$ has been considered as $\overline{U}t$, where $\overline{U}$ is the arithmetic mean of the initial velocity and the velocity at point "M". Since the velocity is proportional to $V^{\frac{1}{6}}$, this assumption should be reasonably accurate. The accuracy of $\frac{\mathrm{d}p}{\mathrm{d}t}$ cannot be readily determined but, from measurements with an inert bubble, an error of 10 % to 20 % is possible. This, together with the uncertainty of any longitudinal variations in concentration within the column, suggests an overall uncertainty of some +30 or 40 % in the value of the mass transfer coefficients. Sievert's Law constant has been taken as 1.76×10^{-3} g atom oxygen $\mathrm{cm}^{-3}\,\mathrm{atm}^{-0.5}$, [11].

The calculated mass transfer coefficients are shown in Figure 10. Reproducible results have been obtained for small bubbles with an equivalent radius of less than 1.2 cm, but for larger bubbles the results showed a greater scatter. The higher values of k_L, for some of these larger bubbles may have been due to the individual bubbles breaking up as they rose in the column. The mean value for the mass transfer coefficient is 0.055 $\mathrm{cm\,s^{-1}}$.

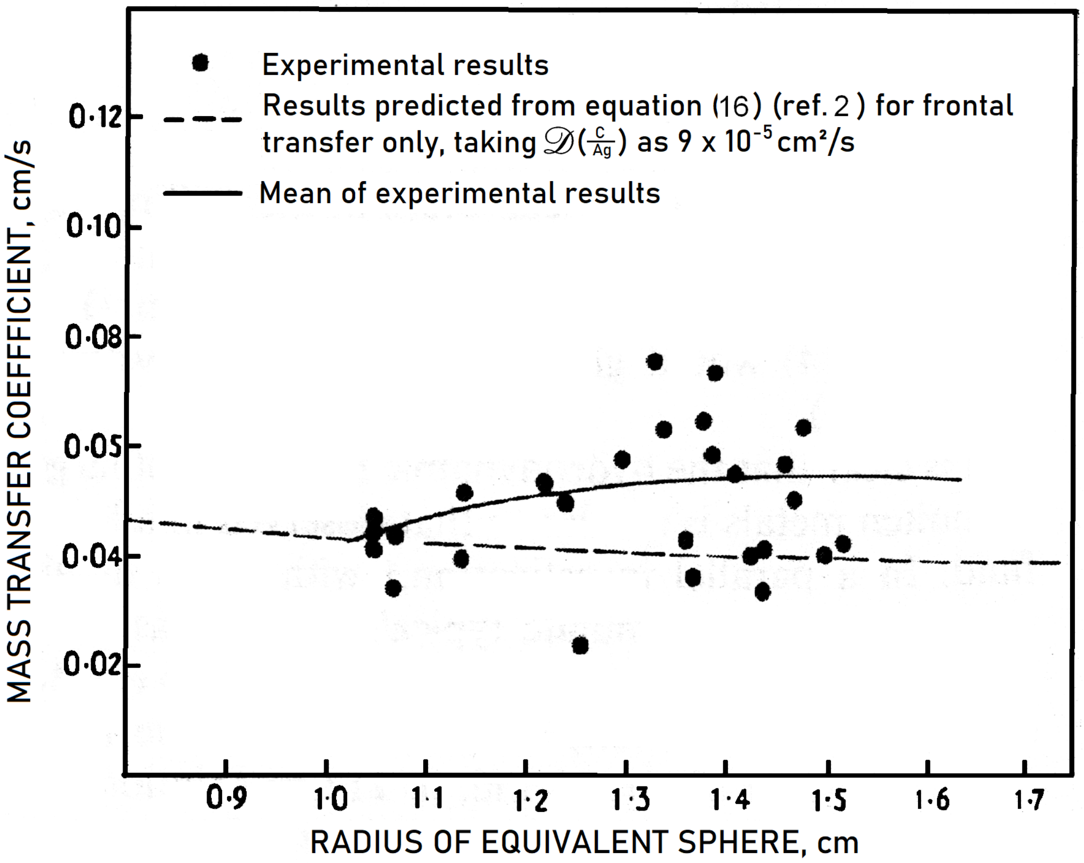

Figure 10: Mass transfer coefficient for various sized bubbles rising in molten silver, (1010 °C)

4. DISCUSSION OF RESULTS

4.1. Rising Velocities

Previous investigators, [10], [12], have found that large gas bubbles rising in water, or other liquids of a similar density, exhibit a spherical cap shape with a spherical front surface and an approximately plane undersurface (Figure 1). Davies and Taylor found that the equation for potential flow, around a sphere in the region close to the forward stagnation point, could be combined with Bernoulli's equation to give the following expression for the rising velocity:

$$U_\infty = \frac{2}{3} \cdot \sqrt{g \cdot R_c} \tag{11}$$

The half-angle subtended at the centre of curvature of typical spherical cap bubbles rising in water is about 50°. In the next section, it is shown that bubbles in mercury have a similar shape, so that Equation 11 may be written in terms of an equivalent radius as:

$$U_\infty = 1.02 \cdot \sqrt{g \cdot r_e} \tag{12}$$

Figure 4 shows the velocities of bubbles rising in mercury and in water. At small volumes, agreement with Equation 12 is satisfactory with both liquids. However, with large bubbles, the constricting effect of the walls reduced the terminal velocity below the predicted value.

Since the velocities in silver were measured in a tube of 7.6 cm i.d., a direct comparison with the velocities obtained for bubbles in mercury is not meaningful. However, as Figure 8 indicates, the results with silver agree reasonably well with those reported by Uno and Kintner for bubbles rising in a column of water of similar diameter, [18]. In view of these results, it can be concluded that neither the surface tension ($\gamma_{Ag} = 920\,\mathrm{dyn\,cm^{-1}}$), nor the density of the fluid ($\rho_{Ag} = 9.5\,\mathrm{g\,cm^{-3}}$), has any noticeable effect on the rising velocity. The effect of viscosity is referred to below.

4.2. Bubble Shapes

The heights of bubbles in mercury obtained from the electrical probe measurements were similar to those in water. On the other hand, the basal radii were 3 mm to 4 mm less than those for similar volume bubbles in water. Since the terminal velocities in the two systems were identical, it is probable that the radii of curvature of the front surfaces were the same in mercury as in water. The smaller basal radius in mercury may well be due to rounding of the trailing edge. Surface-tension forces result in an increase in pressure across the liquid/gas interface at this edge, equivalent to γ/R_E. In view of the similar velocities and shapes of bubbles in mercury and water, it would not be unreasonable to expect that at the trailing edge:

$$\left(\frac{\gamma}{R_E}\right)_{\text{water}} = \left(\frac{\gamma}{R_E}\right)_{\text{Hg}} . \tag{13}$$

Hence:

$$R_E(Hg) = \frac{(\gamma)_{\mathrm{Hg}}}{(\gamma_{\mathrm{water}})} \cdot R_E(\mathrm{water})\,. \tag{14}$$

The 3 mm to 4 mm difference in basal radii could be produced by difference in the radii of curvature at the trailing edge of this same amount. If, for example, the radius of curvature of the trailing edge (R_E) in mercury ($\gamma = 487\,\mathrm{dyn\,cm^{-1}}$) is 4.7 mm, Equation 14 would give 0.7 mm for R_E in water ($72.8\,\mathrm{dyn\,cm^{-1}}$).

It is clear that the hydrodynamic behaviour of large bubbles in molten metals is similar to that observed in a lower density fluid. In a parallel investigation, [8], with fluids of higher viscosities chosen to simulate typical slags, it has been noticed that, at values of up to 100 cP, viscosity has no effect on either the shape or the velocity of the bubble. Above 100 cP, some retardation was observed and, in 212 cP solution, which was the maximum used, the velocities were reduced by some 12 % for small bubbles(r_e =1 cm). The effect was much less for larger bubbles. For example, with an equivalent radius of 2 cm, the decrease in velocity of a bubble was approximately 4 %. The high-viscosity solutions also had the effect of reducing the radius of curvature of the front surface so that the DAVIES and TAYLOR relation (Equation 11) satisfactorily represented the velocities, even in the most viscous solutions tested.

4.3. Passage of Bubbles Across a Slag/Metal Interface

In steelmaking, bubbles have to cross the interface between metal and slag. To investigate the phenomena which occur in such a process, photographic studies were made of bubbles of nitrogen passing from mercury in a variety of aqueous phases. These consisted of distilled water, water acidified with HCl (pH = 2.0) to prevent the formation of oxide films on the mercury surfaces, and water rendered more viscous by the addition of polyvinyl alcohol (57 cP). The bubble was photographed (1000 frames $\mathrm{s^{-1}}$) as it crossed the phase boundary. A typical series of photographs is shown in Figure 11. Initially, a large spherical dome forms (see Figure 11(a)), from which a mercury coated bubble emerges (see Figure 11(b)). The mercury coating ruptures at one point and quickly peels away, and the bubble becomes distorted. The mercury skin which has started to disintegrate in Figure 11(c), has completely disappeared 0.026 s later (see Figure 11(f)). Eventually, out of range of the photographs shown, the bubble breaks up into a central part and a series of small bubbles situated in an annulus around its trailing edge. Several important features merit consideration:

1. a comparison of the spherical dome observed at the mercury/water interface, with the dome of a similar volume bubble in water, shows that the maximum diameter observed in the mercury is some 50 % larger than the basal diameter of the spherical cap bubble. A similar

observation was noted by Davidson and Harrison, [9], on bubbles emerging from a fluidized bed

2. measurement of the distance moved between Figure 11(a) and Figure 11(f) showed that the approximate velocity of a 40 cm^3 bubble passing through the interface was some 30 $\mathrm{cm\,s^{-1}}$. This figure is about 80 % of the normal terminal velocity; the retardation which appears to occur at the interface may be caused by the work necessary to lift the metal into the aqueous phase, and to create the new mercury/water interface around the bubble
3. although much of the mercury surrounding the bubble drains away through the central "umbilical cord", the final peeling away of the mercury coating is accompanied by a cloud of small droplets thrown off the surface of the bubble. The bubbles behave similarly when the water is acidified with HCl or made more viscous with PVA.

4.4. Mass Transfer between Bubbles and Liquids

Davidson and Harrison, [9], and Baird and Davidson, [2] have shown that the rate of mass transfer across a curved surface is given by:

$$\frac{\mathrm{d}n}{\mathrm{d}t} = 4\sqrt{\pi} \cdot (C_b - C_i) \cdot R_c^{\frac{3}{2}} \sqrt{\mathscr{D}} \cdot \sqrt{\int_0^{\alpha} U_s \cdot \sin^2(\alpha)\,\mathrm{d}\alpha}\,. \tag{15}$$

Application of this to the front surface of a spherical cap bubble, for which α is typically around 50°, [2], shows that the mass transfer coefficient may be given by:

$$k_L = 0.82 \cdot r_e^{-\frac{1}{4}} \cdot \mathscr{D}^{\frac{1}{2}} \cdot g^{\frac{1}{4}}\,. \tag{16}$$

Lochiel and Calderbank, [14], obtained a similar expression, though they expressed the coefficient in terms of the actual bubble surface area, and not the area of an equivalent volume sphere. Consequently, a different value of the constant was obtained.

This theory shows reasonable agreement with the experimental results on mass transfer in bubbles rising in aqueous solutions, [8, 2, 14]. The present mass transfer results for oxygen bubbles in silver also compare satisfactorily with the values predicted from the theoretical model (Figure 10). The slightly higher values obtained from experiment are to be expected since they are based on total oxygen transfer, whereas the theory has only allowed for transfer through the front surface. In addition, rippling of the surface, which has been observed with bubbles rising in alcohol, and in certain aqueous solutions, [8], may occur with molten silver, and this would enhance the mass transfer rate.

It has not been directly proved that chemical kinetics have no effect on the rate of absorption of oxygen by silver. But the fact that the values for the mass transfer coefficient derived from the observed rates are somewhat

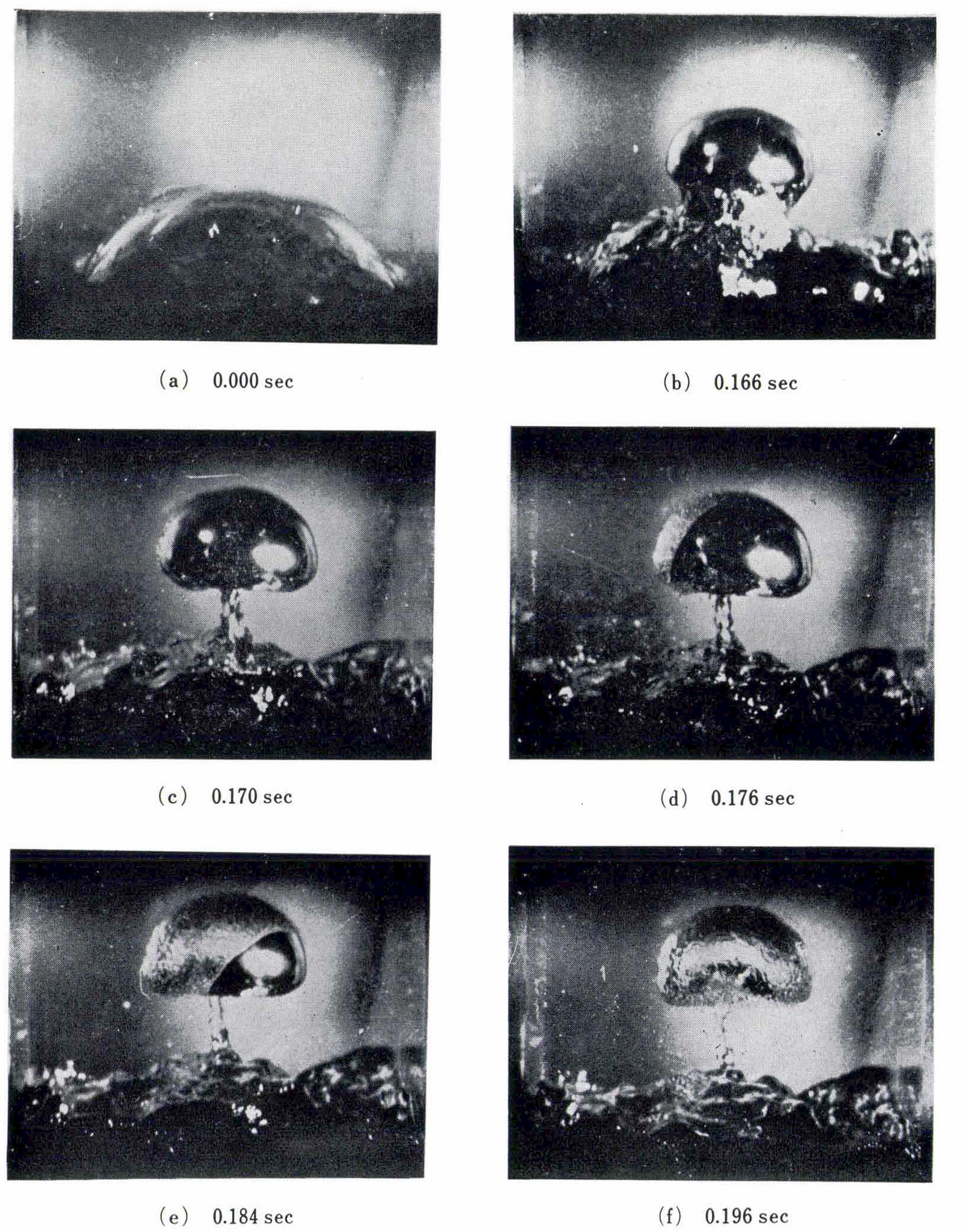

(a) 0.000 sec

(b) 0.166 sec

(c) 0.170 sec

(d) 0.176 sec

(e) 0.184 sec

(f) 0.196 sec

Figure 11: Series of photographs illustrating emergence of 40 cm^3 mercury-coated bubble through mercury/water interface; times relative to (a); add 0.144 s to obtain times from initial bubble appearance;
(a) – formation of spherical dome;
(b) – initial emergence of bubble after 0.166 s;
(c) – start of disintegration of mercury skin, 0.170 s;
(d) – continued disintegration, 0.176 s;
(e) – after 0.184 s;
(f) – complete disappearance of mercury skin after 0.196 s

larger than the values derived theoretically, lends strong support to the view that chemical kinetics are not important, especially since the theoretical Equation 16 holds reasonably for a variety of aqueous media. It is unwise to argue that chemical control is unlikely on general chemical grounds on account of the relatively low temperature of the experiments.

4.5. Interpretation of Industrial Observations

It is interesting to estimate a possible value for the mass-transfer coefficient for bubbles in open-hearth steelmaking, on the assumptions that the bubbles start from the bottom, and that the rate at which carbon monoxide passes into them is controlled by transport in the metal phase. In such circumstances, the rate of transfer of oxygen is likely to be the limiting factor, because the oxygen concentration in the bath is much smaller than the carbon, and the diffusion coefficient of oxygen is less than that of carbon, [4]. For the decarburization of steel by the reaction

$$[\mathrm{O}] + [\mathrm{C}] = \mathrm{CO}\,, \tag{17}$$

an equation similar to Equation 6 may be written for the transfer of oxygen from the steel to the rising gas bubbles. If the head of liquid is substituted for time as the independent variable in the first term, the equation becomes:

$$UP \cdot \frac{\mathrm{d}V}{\mathrm{d}h} + VBU - k_L S V^{\frac{2}{3}} \mathscr{R}\theta \cdot \left(C\,[\mathrm{O}]_i - C\,[\mathrm{O}]_b\right)\,, \tag{18}$$

where U, which equals $\frac{\mathrm{d}h}{\mathrm{d}t}$, may be replaced by an alternative form of Equation 12, giving the velocity in terms of bubble volume:

$$U = 0.80 \cdot g^{\frac{1}{2}} V^{\frac{1}{6}}\,. \tag{19}$$

The resulting expression for the bubble volume in terms of head of liquid has been integrated, [5], to give:

$$\begin{aligned} \sqrt{\frac{V_T}{V_I}} = \frac{k_L S \rho_{\mathrm{Fe}} \mathscr{R}\theta}{0.80 \cdot g^{\frac{1}{2}} V_I^{\frac{1}{2}} \cdot (AW\,[\mathrm{O}]) \cdot 100} \cdot \Bigg[\frac{KH_I}{3 \cdot [\%\mathrm{C}]_i} \cdot \Bigg\{ \left(\frac{H_T}{H_I}\right) - \\ - \left(\frac{H_T}{H_I}\right)^{-\frac{1}{2}} \Bigg\} - \frac{[\%\mathrm{O}]_b}{B} \cdot \Bigg\{ 1 - \left(\frac{H_T}{H_I}\right)^{-\frac{1}{2}} \Bigg\} \Bigg] + \left(\frac{H_T}{H_I}\right)^{-\frac{1}{2}}\,, \end{aligned} \tag{20}$$

where H_T and H_I are the final and initial depths of the bubble below a surface of zero pressure (i.e. they are equal to the actual head of steel plus atmospheric pressure expressed as head of steel).

The observations of Richardson, [17], made during gentle boils (about 0.15 % C lost per hour) in an open-hearth furnace, show that the basal radii of the bubbles, as they break out of the slag, are about 2.5(5) cm, with metal baths about 18 in deep. From laboratory observations made on bubbles emerging from liquid mercury into air, it appears that the dome pushed up by the bubble is some 50 % greater in diameter than the spherical cap itself. Thus, the true basal radius a is nearer 1.7(4) cm. This is related to the volume V_T used in Equation 20 by the equation:

$$a = 0.92 \cdot V^{\frac{1}{3}}\,, \tag{21}$$

where the constant has been taken from the mercury line in Figure 6.
According to the observations made by Brower and Larsen, [7, 6] and Larsen, [13] on gently boiling open-hearth melts with 12 in of metal, the excess oxygen in the bath, over and above that which would be in equilibrium with CO at 1 atm and the carbon in the metal, is about 0.02 wt − % over the range 0.1 % to 1 % C. There is evidence, [1], however, that the excess oxygen observed by Brower and Larsen is rather high (at least for 12 in to 18 in of metal), and it would be more correct to put this value at 0.01 wt − %. For a typical value of $[\%\mathrm{C}]_b$ equal to 0.40, one may reasonably put $[\%\mathrm{O}]_b$ equal to 0.015 %. Since carbon and oxygen cross into the bubbles in equal proportion, $[\%\mathrm{C}]_i$ in Equation 20 is approximately equal to $[\%\mathrm{C}]_b$.
As far as the other variables in Equation 20 are concerned, the initial volume of the bubble when it breaks away from the hearth has been taken as $0.25\,\mathrm{cm}^3$[1]. The bath depth has been taken as 18 in with a 6 in slag cover. Thus, with a hot metal density of $7.2\,\mathrm{g\,cm^{-3}}$ and a slag density of $3.2\,\mathrm{g\,cm^{-3}}$, the values of H_T and H_I are 196.0 and 150.4 cm of steel. The slight change in the bubble volume between the bottom and top of the slag layer, due to the different static pressures at the two positions, has been neglected since it is small compared with the accuracy of the estimate of the bubble volume.
The value of B for molten steel is $6.95 \times 10^{-3}\,\mathrm{atm\,cm^{-1}}$.
The introduction of all these values into Equation 20 leads to a value of the mass transfer coefficient of oxygen to the bubble of $0.08(4)\,\mathrm{cm\,s^{-1}}$.
This value may be compared with a value predicted from the experimental results obtained in this work for oxygen transfer to silver, using Equation 16. This equation shows that:

$$k_{L(\mathrm{O/Fe})} = k_{L(\mathrm{O/Ag})} \cdot \sqrt{\frac{\mathscr{D}_{(\mathrm{O/Fe})}}{\mathscr{D}_{(\mathrm{O/Ag})}}}\,. \tag{22}$$

Taking $\mathscr{D}(\mathrm{O/Ag})_{1000^\circ}$ as $9 \times 10^{-5}\,\mathrm{cm^2\,s^{-1}}$, [15], and $\mathscr{D}(\mathrm{O/Fe})_{1600^\circ}$ as $4 \times 10^{-5}\,\mathrm{cm^2\,s^{-1}}$, [4], and assuming a mean experimental value of $k_L(\mathrm{O/Ag})$ of $0.055\,\mathrm{cm\,s^{-1}}$, then $k_L(\mathrm{O/Fe})$ will be about $0.04\,\mathrm{cm\,s^{-1}}$. This is of the same order as the value obtained above from the observed bubble size.
Predictions based on experiments with single bubbles in silver inevitably ignore effects which may occur when bubbles rise in close proximity to one another. Observations on the open-hearth furnace show a range of bubble sizes, and it is not known to what extent bubbles coalesce. Nevertheless, the degree of agreement indicated above makes it seem reasonable that mass transfer of CO into bubbles in the open-hearth is transport-controlled.

---

[1] If $0.1\,\mathrm{cm}^3$ or $0.5\,\mathrm{cm}^3$ are taken as the volume on release, the derived value of k_L is only raised or lowered by 15 %.

Appendix

A. DEVIATIONS OF MEAN VELOCITY AND EQUIVALENT RADIUS FROM INSTANTANEOUS VALUES

The measurements of bubble velocity which are shown in Figure 4 of the paper represent the mean velocity over a fixed height of the column $\frac{h_0}{T}$ plotted against the mean equivalent radius, which is based on the arithmetic average volume in the bubble at the lower position, and at the top of the column. It is important to see how these would differ from the instantaneous values of the two variables. This comparison can be readily made if the instantaneous velocity is assumed to be proportional to the equivalent volume raised to an arbitrary power w:

$$U = -\frac{\mathrm{d}h}{\mathrm{d}t} = M \cdot V^w \,. \tag{A.1}$$

Since HV is constant, Equation A.1 can be integrated over time T to give:

$$T = \frac{H_I^{1+w} - H_T^{1+w}}{(1-w) \cdot M \cdot (H_I V_I)^w} \,. \tag{A.2}$$

The arithmetic mean volume V_{AV}, which is equivalent to $\frac{V_T + V_I}{2}$, is given by:

$$V_{\mathrm{AV}} = \frac{V_I}{2} \cdot \left(1 + \frac{H_I}{H_T}\right) \,. \tag{A.3}$$

If $V^\star$ is the instantaneous volume given by Equation A.1 for the particular value of the instantaneous velocity U equal to the mean velocity, then:

$$\frac{h_0}{T} = M \cdot V^{\star w} \,. \tag{A.4}$$

Substitution of Equation A.3 and Equation A.4 into Equation A.2 gives:

$$\frac{V_{\mathrm{AV}}}{V^\star} = \frac{1 + \left(\frac{H_T}{H_I}\right)^{-1}}{2} \cdot \left[\frac{1 - \left(\frac{H_T}{H_I}\right)^{1-w}}{(1+w) \cdot \left(1 - \frac{H_T}{H_I}\right)}\right]^{\frac{1}{w}} \,.$$

The value of w for a spherical cap bubble is $\frac{1}{6}$. In these experiments of bubbles rising in mercury, the top pressure was atmospheric, and the depth of the column was 48 cm, so that H_T and H_I were 76 and 124 cm Hg respectively. This gives a value for $\frac{V_{\mathrm{AV}}}{V^\star}$ of 1.08, and the true volume $V^\star$ corresponding to the instantaneous velocity U is about 8 % less than the arithmetic average. In terms of equivalent radius, the curves shown in Figure 4 overestimate the value of this radius, corresponding to the instantaneous velocity by at most

3 %. For bubbles rising in fluids of lower density than mercury, the ratio $\frac{H_T}{H_I}$ is likely to be close to unity and the error less. However, if experiments are carried out with the surface of the liquid held under a vacuum, the value of $\frac{H_T}{H_I}$ could be small ($\ll 1$) and, in this case, the use of an arithmetic average volume might lead to significant errors.

References

[1] The United Steel Companies Ltd, Rotherham, private communication.

[2] M. H. I. Baird and J. F. Davidson. Gas absorption by large rising bubbles. *Chemical Engineering Science*, 17(2):87–93, 1962.

[3] E. H. Baker. Dept. of Metallurgy, Imperial College of Science and Technology, private communication.

[4] G. Belton. School of Metallurgical Engineering. University of Pennsylvania, Philadelphia, private communication.

[5] A. V. Bradshaw, W. G. Davenport, and D. H. Wakelin. Interaction of both Bubbles and Gas Jets with Liquids. In A. W. D. Hills, editor, *Heat and mass transfer in process metallurgy*, John Percy Research Group Symposium, pages 207–240, Imperial College, London, 1967. Institution of Mining and Metallurgy.

[6] T. E. Brower and B. M. Larsen. Oxygen in Liquid Open-hearth Steel-Effect of Special Additions, Stirring Methods and Tapping. *Transactions of the American Institute of Metallurgical Engineers*, 172:164–175, 1947.

[7] T. E. Brower and B. M. Larsen. Oxygen in Liquid Open-hearth Steel-Oxygen Content During the Refining Period. *Transactions of the American Institute of Metallurgical Engineers*, 172:137–163, 1947.

[8] W. G. Davenport, F. D. Richardson, and A. V. Bradshaw. Spherical cap bubbles in low density liquids. *Chemical Engineering Science*, 22(9):1221–1235, 1967.

[9] J. F. Davidson and D. Harrison. *Fluidized particles.* Cambridge University Press, 1 edition, 1963.

[10] R. M. Davies and G. I. Taylor. The mechanics of large bubbles rising through extended liquids and through liquid tubes. *Proceedings of the Royal Society of London. Series A. Mathematical and Physical Sciences*, 200(1062):75–390, 1950.

[11] C. Diaz, C. R. Masson, and F. D. Richardson. Electrochemical Determination of Oxygen in Liquid Silver. *Transactions of the Institutions of Mining and Metallurgy*, 75:183–185, 1966.

[12] W. L. Haberman and R. K. Morton. An experimental investigation of the drag and shape of air bubbles rising in various liquids. Technical Report 802, Navy Department, The David W. Taylor Model Basin Washington 7, D.C., 1953.

[13] B. M. Larsen. A new look at the open hearth process. Technical Report 1, National Open Hearth Steel Committee, American Institute of Mining, Metallurgical, and Petroleum Engineers, 1956.

[14] A. C. Lochiel and P. H. Calderbank. Mass transfer in the continuous phase around axisymmetric bodies of revolution. *Chemical Engineering Science*, 19(7):471–484, 1964.

[15] E. A. Mizikar, R. E. Grace, and N. A. Parlee. Diffusion of Oxygen in Liquid Silver. *Transactions of American Society for Metals*, 56:101–106, 1963.

[16] R. D. Pehlke and A. I. Bement. Mass transfer of hydrogen between liquid aluminium and bubbles of argon gas. *Transactions of the American Institute of Metallurgical Engineers*, 224:1237–1242, 1962.

[17] F. D. Richardson. Rates of slag-metal reactions and steelmaking processes. *Iron and Coal Trades Review*, 183:1105–1115, 1961.

[18] S. Uno and R. C. Kintner. Effect of wall proximity on the rate of rise of single air bubbles in a quiescent liquid. *Journal of the American Institute of Chemical Engineers*, 2(3):420–425, 1956.